Supplementary Information: Coupling Isotachophoresis with Affinity Chromatography for Rapid and Selective Purification with High Column Utilization Part II: Experimental Study

Viktor Shkolnikov, Juan G. Santiago*

*Department of Mechanical Engineering, Stanford University, Stanford, CA 94305, USA. * Tel: 650-723-5689; Fax: 650-723-7657; E-mail: juan.santiago@stanford.edu*

We here present additional information on the following topics:

SI 1. Extraction of analyte from the TE reservoir in semi-infinite injection ITP

In the main text of Part I of this two-paper series, we focused our analysis on the case of finite sample injection[1], wherein sample is introduced into a finite section of the channel and bounded by LE on the right side and pure TE on the left side (e.g., pure TE in the reservoir). Finite sample injection enables a designer to fairly easily collect all of the target analyte into the ITP zone prior to reaching the affinity region. See for example Bocek et al.[2] and Marshall[3] for analyses around requirements to focus all sample in ITP for finite injection. The arrangement of finite injection (i.e., requirement to "sandwich" the sample between pure LE and TE[4]) makes it less convenient experimentally, but the method is simpler to analyze and describe, so we used it in our model in Part I.

We here briefly analyze the case of a so-called semi-infinite injection.[1] In semi-infinite injection, the sample is mixed with TE and this mixture is placed into a large reservoir, while the channel and affinity column are filled with pure LE. We present an estimate of the required length to extract most of the sample from the reservoir using semi-infinite injection.

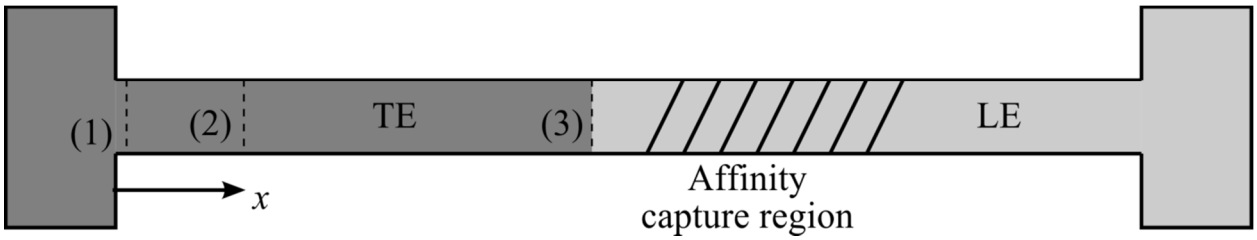

Figure S-1. Schematic of a channel with LE and TE reservoirs in which ITP with semi-infinite injection is performed. Labeled numerically are three planes through which the flux of analyte is analyzed. We analyze this problem to study of the influence of the length between the TE reservoir and the affinity capture region (cross hatched) on the fraction of sample extracted. Planes (1) and (2) are fixed, while Plane (3) is located at and moves with the LE-TE interface. Plane (1) is located is located just inside the channel near the TE reservoir and experiences the same concentration of analyte as in the TE reservoir.

We derive an estimate for the length of channel from the TE reservoir to the affinity region that is necessary to nearly completely extract an analyte from the sample and TE mixture in the TE reservoir. The analysis is an aid to designers as it determines how far downstream from the input reservoir an experimentalist should place the affinity column. Our analysis follows a similar form of that presented by Persat et al. for species exiting a reservoir[5] but is specific to our situation where the species are focusing in ITP.

We begin by noting that in the semi-infinite injection scheme the amount of analyte leaving the TE reservoir, ϕ_{P1} (i.e., passing through Plane 1 located a small distance into the channel as shown in Figure S-1) is given by

$$\phi_{P1} = A_C \mu_{a,R} E_R c_{a,R}, \tag{1}$$

where A_C is the cross sectional area of the channel, $\mu_{a,R}$ is the mobility of the analyte in the reservoir, E_R is the effective electric field near the entrance of the channel, and $c_{a,R}$ is the concentration of analyte in the reservoir. We assume that the reservoir is well mixed (analyte always uniformly distributed in the reservoir) including near the entrance of the channel. Equation (1) can be rewritten using Ohm's law as

$$\phi_{P1} = A_C \mu_{a,R} \frac{I}{A_C \sigma_R} c_{a,R}, \tag{2}$$

where I is the current through the system, and σ_R is the conductivity of the TE reservoir. We assume that the reservoir is well buffered and that the conductivity of the TE reservoir does not change during the ITP process. In this convention and for anionic ITP, I is negative. The amount of analyte leaving the TE reservoir is proportional to the decrease in concentration of analyte in the reservoir,

$$\frac{dc_{a,R}}{dt} V_R = -\phi_{P1} = -\frac{\mu_{a,R} I}{\sigma_R} c_{a,R}, \tag{3}$$

where V_R is the volume of the reservoir. We solve the differential equation (3) subject to the initial condition of $c_{a,R} = c_{a0,R}$ at $t = 0$, which yields

$$c_{a,R} = c_{a0,R} \exp\left(-\frac{\mu_{a,R} I}{V_R \sigma_R} t \right). \tag{4}$$

The rate of accumulation of analyte at the LE-TE interface[2] is given by

$$\frac{dn_{a,LE-TE}}{dt} = A_C c_{a,TE} \left(\mu_{a,TE} E_{TE} - u_{ITP} \right), \tag{5}$$

where $n_{a,LE\text{-}TE}$ is the amount (e.g., number of moles) of analyte in the LE-TE interface, $c_{a,TE}$ is the concentration of analyte in the adjusted TE, $\mu_{a,TE}$ is the mobility of the analyte in the adjusted TE, E_{TE} is the electric field in the adjusted TE (assumed to be uniform), and u_{ITP} is the velocity of the LE-TE interface. Further, we note that amount of analyte traveling through Plane 1 in Figure S-1 is equal to that traveling through Plane 2 as no accumulation occurs between these two planes. The amount of analyte traveling through Plane 2 is given by

$$\phi_{P2} = A_C \mu_{a,TE} E_{TE} c_{a,TE}. \tag{6}$$

Combining (5) with (6) and noting that $\phi_{P1} = \phi_{P2}$ we obtain

$$\frac{dn_{a,LE-TE}}{dt} = A_C \frac{\phi_{P1}}{A_C \mu_{a,TE} E_{TE}} \left(\mu_{a,TE} E_{TE} - u_{ITP} \right). \tag{7}$$

Combining (7) with (3) we obtain

$$\frac{dn_{a,LE-TE}}{dt} = c_{a,R} \frac{\mu_{a,R} I}{\sigma_R \mu_{a,TE} E_{TE}} \left(\mu_{a,TE} E_{TE} - u_{ITP} \right). \tag{8}$$

We then simplify (8), recalling that $u_{ITP} = \mu_{TEion,TE} E_{TE}$ (where $\mu_{TEion,TE}$ is the mobility of the TE ion in the adjusted TE)[6]

$$\frac{dn_{a,LE-TE}}{dt} = c_{a,R} \frac{\mu_{a,R}}{\mu_{a,TE}} \frac{I}{\sigma_R} \left(\mu_{a,TE} - \mu_{TEion,TE} \right). \tag{9}$$

Next, we combine (9) with the solution for the analyte concentration in the TE reservoir (4) to obtain

$$\frac{dn_{a,LE-TE}}{dt} = c_{a0,R} \exp\left(-\frac{\mu_{a,R} I}{V_R \sigma_R} t \right) \frac{\mu_{a,R}}{\mu_{a,TE}} \frac{I}{\sigma_R} \left(\mu_{a,TE} - \mu_{TEion,TE} \right). \tag{10}$$

We solve the differential equation (10) subject to the initial condition $n_{\mathrm{a,LE\text{-}TE}} = 0$ at $t = 0$ giving

$$n_{a,LE-TE} = c_{a0,R} \frac{V_R \sigma_R}{\mu_{a,R} I} \left(\frac{\mu_{a,R}}{\mu_{a,TE}} \frac{I}{\sigma_R} \left(\mu_{a,TE} - \mu_{TEion,TE} \right) \right) \left(1 - \exp\left[-\frac{\mu_{a,R} I}{V_R \sigma_R} t \right] \right). \tag{11}$$

We simplify (11), recalling $c_{\mathrm{a0,R}} V_{\mathrm{R}} = n_{\mathrm{a0,R}}$ and obtain

$$\frac{n_{a,LE-TE}}{n_{a0,R}} = \left(\frac{\mu_{a,TE} - \mu_{TEion,TE}}{\mu_{a,TE}} \right) \left(1 - \exp\left[-\frac{\mu_{a,R} I}{V_R \sigma_R} t \right] \right). \tag{12}$$

We note that ITP velocity can be written as

$$u_{ITP} = \frac{I \mu_{LEion,LE}}{A_C \sigma_{LE}}, \tag{13}$$

and we recast equation (12) in terms of the distance from the TE reservoir, x, that the LE-TE interface has traveled. We obtain

$$\frac{n_{a,LE-TE}}{n_{a0,R}} = \left(\frac{\mu_{a,TE} - \mu_{TEion,TE}}{\mu_{a,TE}} \right) \left(1 - \exp[\zeta] \right), \tag{14}$$

where

$$\zeta = x \frac{\mu_{a,R}}{\mu_{LEion,LE}} \frac{\sigma_{LE}}{\sigma_R} \frac{A_C}{V_R}. \quad (15)$$

We see that the fraction of extracted analyte focused into the LE zone, $n_{a,LE\text{-}TE}/n_{a0,R}$ is limited by species mobilities, ratio of LE buffer to TE reservoir conductivity, the volume of TE reservoir, the cross sectional area of the channel, and the distance from the TE well to the point of interest (i.e., the affinity region).

The mobilities term in the first brackets in equation (14) limits the maximum amount of analyte which can be extracted from the TE well. We see that there is a tradeoff between the amount which can be extracted from the TE well and the degree to which we can separate the extracted substance from a contaminant, co-ionic species not focused in ITP. For a high degree of separation between focused target and unfocused contaminant, the TE ion mobility should be close to that of the target (making the TE ion significantly faster than a contaminant). As per equation (14), however, this limits the fraction of target that we can extract from the reservoir.

For our experiments we chose HEPES for the TE ion as an acceptable tradeoff between separation from contaminants and fraction of sample removed from the reservoir. HEPES has been demonstrated to exclude PCR inhibitors from blood and the HEPES ion itself seems to not inhibit PCR.[1,7] Blood is, of course, a highly clinically relevant biological sample and PCR an important downstream assay. For our buffer conditions, we calculate (using SPRESSO[8]) that the HEPES anion mobility in the adjusted TE was -13 x 10^{-9} $m^2V^{-1}s^{-1}$, while the DNA mobility[9] was approximately -25 x 10^{-9} $m^2V^{-1}s^{-1}$. Based on term in the first brackets in equation (14) this gives us a maximum extraction efficiency of about 44%.

We next consider the term in the second brackets in equation (14). This term dictates at what distance along the channel a certain fraction of analyte is extracted. Hence it dictates the location in the channel where we should place the affinity region. We estimate that for our experimental setup, the term in the second brackets of (14) was about 0.25, giving an overall ITP extraction efficiency, $n_{a,LE\text{-}TE}/n_{a0,R}$, of about 10%.

We note that the semi-infinite injection model can, given sufficient length between sample reservoir and AC column, well approximate the finite injection ITP configuration. For trace analytes (as we consider) and open bore column lengths sufficient to focus by 50x or more, the concentration of target focused in the ITP zone is much larger than the concentration of analyte migrating through the adjusted TE zone. Therefore, most of the reaction product is determined by ITP-focused analyte and not the low concentration inlet flux. Further, ITP-aided AC capture drastically speeds up the capture process. Therefore, the amount of analyte accumulated in the ITP zone prior to its arrival at the AC column is much larger than the amount of analyte which accumulates at the ITP zone during capture.

SI 2. Calibration of Cy5 fluorescence to DNA concentration

We performed a calibration relating DNA concentration in our system and measured fluorescence intensity. We performed this calibration without ITP and by simply filling the entire capillary with a known, uniform concentration of DNA. The calibration relates Cy5 fluorescence in our optical system and Cy5-labeled DNA concentrations of 10 nM to 10 μM. We quantified the fluorescence with the epifluorescence microscope setup described in Section 2.1 of the main text. We then performed a proportional fit between observed fluorescence and DNA concentration.

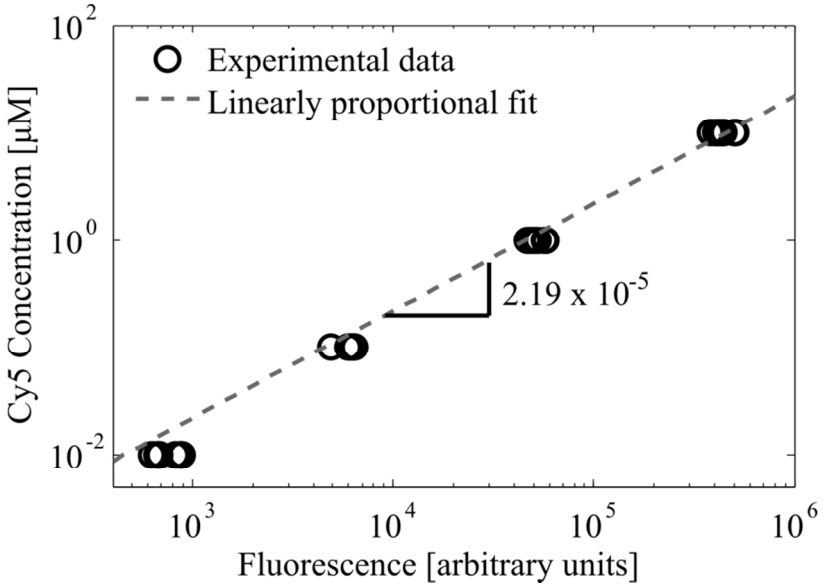

Figure S-2. Plot of Cy5 fluorescence and DNA concentration from 10 nM to 10 μM and proportional fit between Cy5 fluorescence and DNA concentration. The slope of the proportional fit is 2.19 x 10^{-5} μM/(arbitrary unit). The coefficient of determination for the proportional fit is $R^2 = 0.98$.

We observed that our GMA-EDMA PPM enhances significantly the fluorescence of Cy5 labeled DNA. For example, see Figure S-3 where we used pressure driven flow to fill a solution of Cy5 into the capillary and image the region near the boundary of the PPM zone. There is a considerable difference in Cy5 fluorescence between the free solution and the PPM. We hypothesize that this may be due to higher index of refraction of the PPM compared to the surrounding media (water). The refractive index of GMA-EDMA monolith may be close to that of poly(methyl methacrylate) plastics, which have a reported value of 1.487 at 670 nm.[10] We hypothesize the increase in fluorescence could also be caused in part by electronic interaction between the double bonds in the Cy5 dye and those on the PPM surface.[11,12] In any case, the ratio of fluorescence intensity between the PPM and the free solution was 1.74. We accounted for this increase in fluorescence in the PPM in the calculations of probe density N and bound target concentration, n.

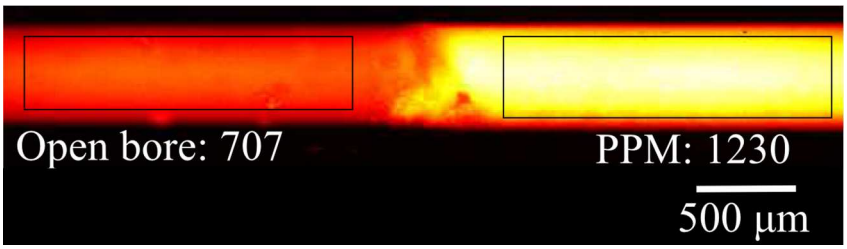

Figure S-3. Cy5 fluorescence intensity near the interface of the open bore section of the capillary and the section with the porous polymer monolith (PPM). For this experiment we filled the capillary and the PPM inside the capillary with a solution of Cy5 labeled DNA using pressure driven flow. The mean fluorescence intensity in the free solution region was 707 (arbitrary units), while that in the PPM was 1230 (arbitrary units). The black rectangles indicate the areas that were averaged for these estimates.

SI 3. Synthetic DNA oligo sequences used

Target sequence:			
Sequence:	5'-CTCTGAACGGTAGCATCTTGACAAC-3'		
Modification:	5' Cy5		
ΔG_{self} (kcal/mol)	0.0		
$T_{m\ self}$ (ºC)	19.1		
Secondary structure	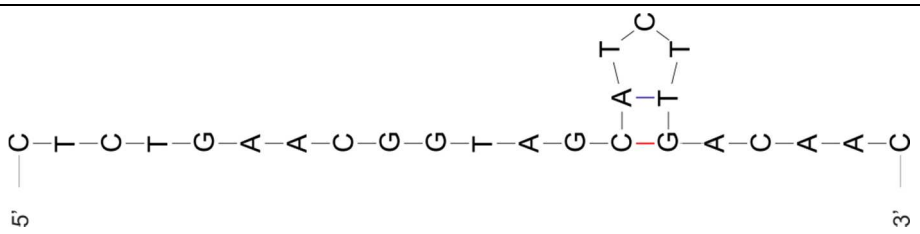		
Calculation conditions	Temperature (ºC)	Na^+ concentration (M)	Mg^{2+} concentration (M)
	20	0.2	0

Probe sequence:			
Sequence:	5'-GTTGTCAAGATGCTACCGTTCAGAG-3'		
Modification:	5' C12-amine		
ΔG_{self} (kcal/mol)	0.3		
$T_{m\ self}$ (ºC)	15.0		
Secondary structure	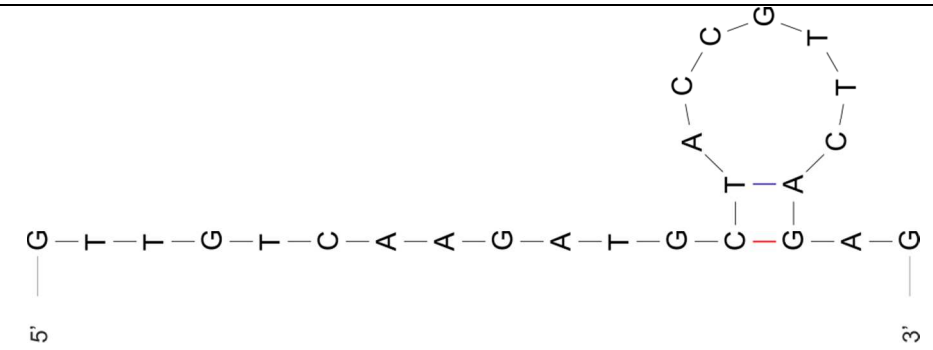		
Calculation conditions	Temperature (ºC)	Na^+ concentration (M)	Mg^{2+} concentration (M)
	20	0.2	0

<table>
<tr><td colspan="5">Hybrid:</td></tr>
<tr><td>ΔG_{hybrid} (kcal/mol)</td><td colspan="4">-35.6</td></tr>
<tr><td>$T_{m\ hybrid}$ (ºC)</td><td colspan="4">63.2</td></tr>
<tr><td>Structure</td><td colspan="4"> 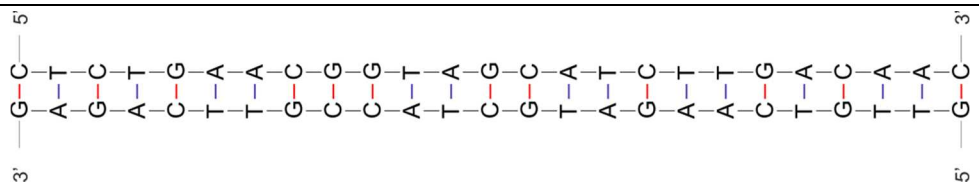
</td></tr>
<tr><td>Hybridization temperature dependence</td><td colspan="4"> 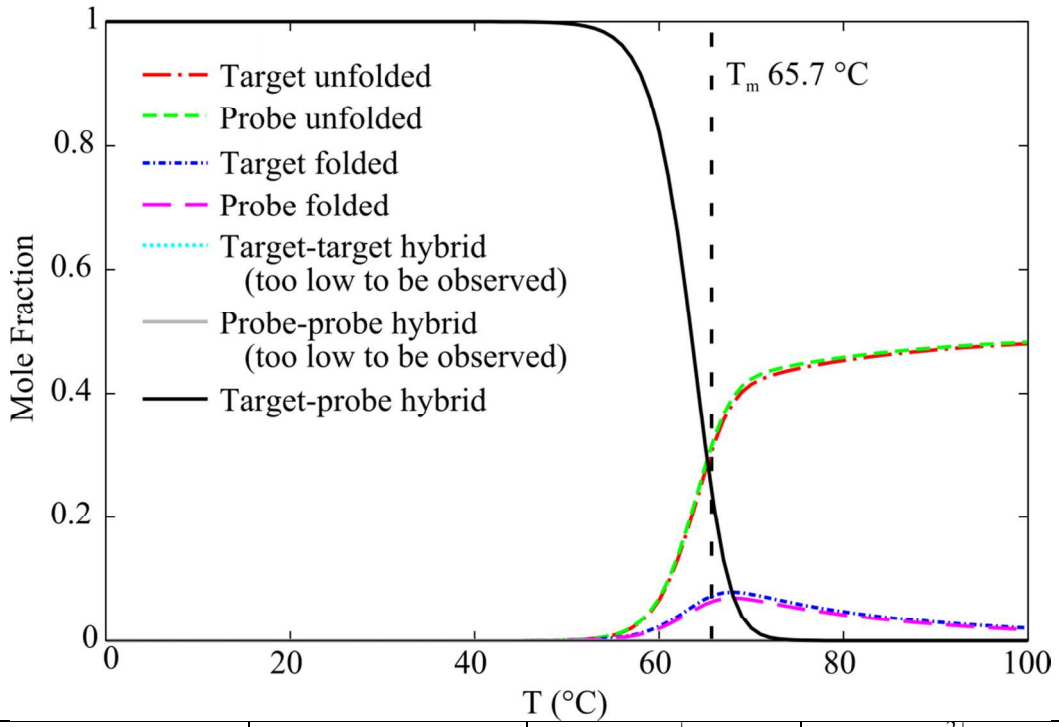
</td></tr>
<tr><td rowspan="2">Calculation conditions</td><td>Temperature (ºC)</td><td>Strand concentration (nM)</td><td>Na^+ concentration (M)</td><td>Mg^{2+} concentration (M)</td></tr>
<tr><td>20</td><td>100</td><td>0.2</td><td>0</td></tr>
</table>

We calculated ΔG, T_m, and sequence secondary structure and hybrid structure using mFold (State University of New York at Albany)[13] at the conditions indicated. While the solution composition is not the same as that used in our ITP-AC experiments, the solution ionic strength is matched as closely as possible. Additionally, mFold calculations assume that the hybridization occurs in solution, not on a surface. We performed an initial calculation of the dissociation constant K_d using the Van't Hoff equation[14],

$$K_d = \exp\left(\frac{\Delta G_{hybrid}}{RT}\right) \tag{16}$$

to be 3 x 10^{-27} M. From this and the measurement of the probe density N, we estimated β to be 1 x 10^{-22}. We believe that this is an extremely low value for a dissociation constant, and is likely

due to the overestimation of the absolute value of ΔG of hybridization by mFold for our conditions. Levicky and Horgan also report similarly large values for dissociation constants of DNA oligonucleotides of similar sizes and for similar ionic strengths for bulk solution hybridization.[15] However, Levicky and Horgan also report surface hybridization dissociation constants that are significantly higher than those for bulk solution hybridization for similar oligonucleotides.[15]

Due to these difficulties in predicting K_d values, we here chose to estimate the expected order of magnitude of the surface hybridization K_d using published experimental values for oligonucleotides under similar hybridization conditions on a surface. For example, Stevens et al. found $K_d < 10^{-11}$ M for a 21 nt oligonucleotide hybridized on 0.75 μm paramagnetic latex particles in 100 mM ionic strength solution at 20°C.[16] Similarly, Okahata et al. found K_d to be 2.5×10^{-11} M for a 30 nt oligonucleotide hybridized on a gold plated quartz crystal microbalance surface in 10 mM ionic strength solution at 20°C.[17] Since the value of K_d strongly decreases with ionic strength,[17] we conservatively expect a K_d of at most 10^{-11} M for our experimental conditions (order 100 mM ionic strength). From this and the measurement of the probe density N, we estimated β to be 3×10^{-7}. We note that for our ITP-AC conditions, the model predictions are very weak functions of β for $\beta < 10^{-5}$ (see Part I, Figure 4). For example, a factor of 10 change in K_d results in less than 1 % change in capture efficiency in this range of β.

SI 4. Measurement of PPM void fraction

We measured the void fraction of the PPM by obtaining the geometric volume of the PPM (i.e., volume of the cylindrical PPM as determined by the capillary inner diameter) and the true volume of the polymer structure. The void fraction, φ, is then given by

$$\varphi = \frac{V_{geom} - V_{solid}}{V_{geom}}, \tag{17}$$

where V_{geom} and V_{solid} are the geometric and true volumes respectively. We measured the volume of the polymer structure by measuring the volume of water it displaced.

During these experiments, we first measured the axial length of the PPM inside the micropipette capillary using a vernier caliper. We calculated the geometric volume of the PPM using this length and the inside diameter of the capillary (provided by the manufacturer). We then slowly filled the PPM with a slug of water of known volume and measured the length of the slug. Using this length and inside diameter of the capillary, we calculated the volume of water after it was displaced by the PPM. We obtained the volume of the solid by subtracting this volume from the initial volume of water. Using this method we obtained a PPM void fraction of 0.8.

SI 5. Image of custom built capillary setup

We performed ITP-AC experiments in a custom built capillary setup (shown in Figure S-4), which interfaced LE and TE reservoirs to the capillary with the PPM. The TE reservoir was fabricated via stereolithography (FineLine Prototyping, Raleigh, NC) from WaterShed XC 11122 and fitted with 1/4-28 female threads to mate to 1/4-28 nut and ferrule from Idex Health & Science (Oak Harbor, WA). The LE reservoir consisted of a Idex Health & Science 90 degree bend fitting (female to female threads). The capillary outer diameter was 1 mm. Custom machined acrylic brackets served to secure reservoirs and electrodes in place during experiments.

The 500 µm inner diameter capillary had 1 to 3 cm long GMA-EDMA PPM structures polymerized inside of it. The PPM was covalently attached to the capillary wall. We functionalized the surface of the PPM with 25 nt DNA probe complimentary to the target. To initiate ITP-AC, we applied current to the capillary using platinum electrodes dipped into LE and TE reservoirs.

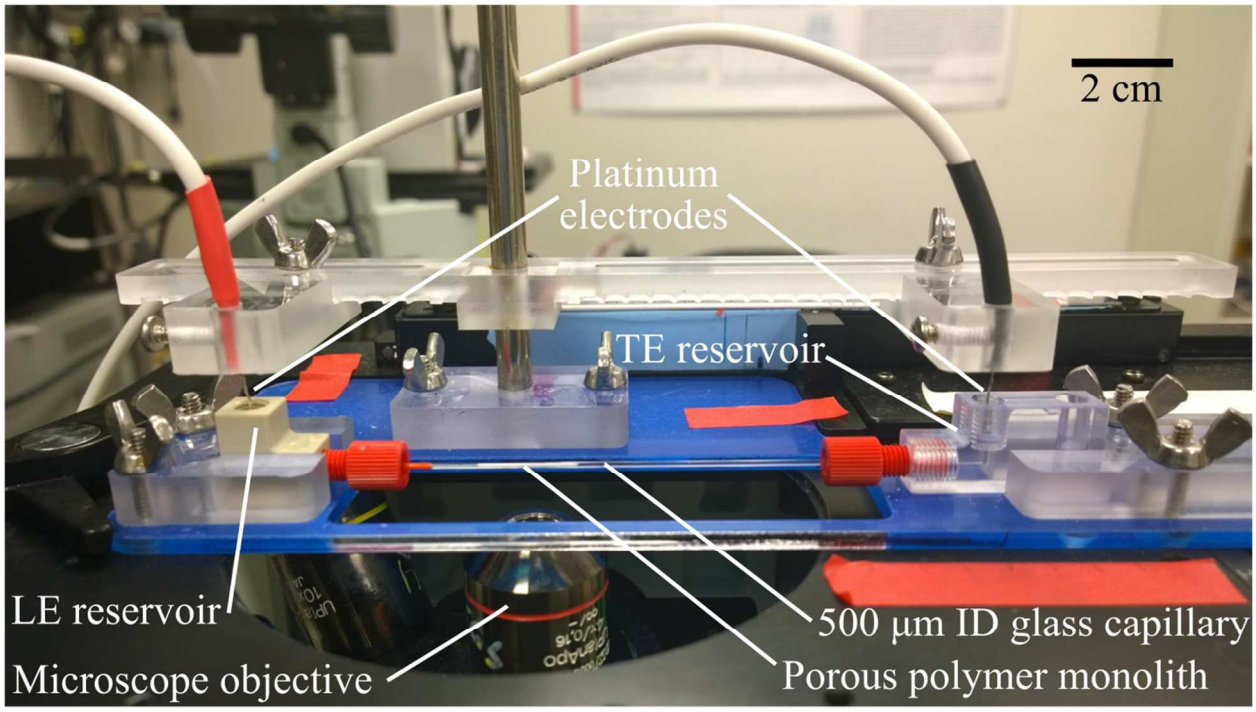

Figure S-4. Image of custom-built capillary setup consisting of LE reservoir, 500 µm inner diameter borosilicate glass capillary with GMA-EDMA PPM, and a TE reservoir. Platinum electrodes were dipped into the LE and TE reservoirs to apply current through the capillary.

SI 6. Choice of porous polymer monolith chemistry, synthesis, and functionalization

SI 6.1 Choice of porous polymer chemistry

Affinity chromatography columns require surfaces to which affinity ligands can be readily bound, but which provide minimal non-specific binding of contaminants. Reproducible and robust affinity chromatography experiments with aqueous solutions also benefit from sufficiently hydrophilic surfaces. We chose a polymerization chemistry which incorporates the monovinyl monomer, GMA, which has an epoxide functional group. The epoxide group on GMA is known to be highly reactive to primary amines on biopolymers such as nucleic acids,[18,19] and proteins,[20-22] and other well-known affinity ligands.[23] Furthermore, GMA-EDMA polymers exhibit little non-specific binding with nucleic acids. GMA-EDMA PPMs also are sufficiently hydrophilic and are easy to use with aqueous solutions. Lastly, methacrylate PPM structures are highly scalable and have been synthesized in both microfluidic[24-27] and 8 L scale formats.[28]

We cross-linked GMA with EDMA via a free radical, UV-initiated polymerization in the presence of MeOH and hexane as solvents, with AIBN as photoinitiator.[29] We chose photo-, rather than thermal-initiation to be able to lithographically define regions of PPM. Ability to lithographically define PPM regions helps incorporate PPMs in prescribed, finite sections of capillaries or within microfluidic chips.[24-27]

SI 6.2 Polymethacrylate porous polymer monolith (PPM) synthesis

Both EDMA and GMA were received with polymerization inhibitors, which we removed by passing through columns packed with inhibitor removing media. We then mixed the photo initiator AIBN (126 mM), GMA (12% v/v), EDMA (8% v/v), MeOH (64% v/v) and hexane (16% v/v) in a polypropylene vial. We injected a slug of this polymerization solution into already prepared, dry, micropipette capillaries with vinylized walls.

We vinylized the walls of the capillaries by placing the capillaries in a solution of 30% (v/v) TSPM, 70% (v/v) acetone solution overnight and then flushing the remaining solution with air.[27] The capillary walls were vinylized to ensure covalent attachment of the polymer to the capillary wall, and thus avoid channeling.[27] We then irradiated samples using a 12 W, ~405 nm peak wavelength UV lamp (Chauvet, Sunrise, FL) at 12 cm exposure distance for 2 h. After polymerization, we flushed the samples with air to remove unreacted monomers and solvents, and dried at 20ºC under approximately 93 kPa vacuum for 30 min. This resulted in 1 to 3 cm long GMA-EDMA PPM structures bound to the capillary wall with approximately 80% (measured) void fraction and order 2 μm pores (see Figure 1b in the main text and Section SI 4). This ensured that the porous affinity region had small hydrodynamic resistance, facilitating filling the system with LE buffer, and later the elution buffer without the need for high pressure pumps.

SI 6.3 Probe DNA immobilization on PPM

We prepared DNA immobilization solution consisting of 3X SSC buffer (450 mM sodium chloride, 45 mM trisodium citrate), 2 mM SDS and 250 μM 5' amine modified synthetic oligo DNA.[19] We slowly injected a slug of this immobilization solution into the micropipette capillaries with the PPM inside. We then placed micropipette capillaries in a water bath at 70ºC for 2 h. We then flushed each capillary with 2 ml of DI water (roughly 500 column volumes) and dried at 70ºC under about 93 kPa gauge vacuum for 1 h.

We estimated the resulting volumetric density of immobilized DNA by immobilizing 5' amine, 3' Cy5 modified synthetic oligo DNA, measuring the resulting fluorescence intensity, comparing the result to a Cy5 labeled DNA fluorescence signal calibration (see Section SI 2). We estimate the volumetric density of immobilized DNA to be about 30 μM. This resulted in total column capacity of 6 to 24 x 10^{-11} moles of target or for 100 nt target 2 to 6 μg and for 1000 nt target 20 to 60 μg of target capacity.

For a rough estimate of surface density of immobilized DNA, we roughly approximate the PPM (see Figure 1b) as consisting of a cubic closed pack crystal of spheres with 1 μm diameter. This provides an estimate of immobilized DNA surface density of 1.2 x 10^{-12} molecules cm^{-2}. DNA probe surface densities of around 2 x 10^{-12} molecules cm^{-2} have been shown to provide high (>60%) hybridization efficiencies, while higher probe surface densities decrease hybridization efficiency.[30] Peterson et al. attribute this to repulsive electrostatic and steric interactions that increase with increased probe density.[30]

SI 7. Choice of buffer chemistry for ITP-AC

In our final experiments the LE buffer consisted of 250 mM HCl and 500 mM Tris. The TE buffer as placed in the TE well consisted 25 mM HEPES, 50 mM Tris, and varying amounts of target and/or contaminating species. The LE ion (here chloride) maintains its concentration throughout the experiment. The LE buffer governs the concentration of the adjusted HEPES anion concentration (i.e., the TE ion concentration behind the LE-TE interface).[6,31,32] The adjusted TE ion concentration is generally roughly 0.5-0.8 that of the LE ion.[32] In our experiments the adjusted TE concentration was calculated to be 150 mM using an electrokinetic simulation software SPRESSO.[8]

We chose a relatively high LE concentration to ensure that the focused DNA target was in a buffer of high ionic strength. This suppresses the characteristic lengths of electric double layers associated with the surface of the PPM and the immobilized nucleic acids.[33] Increasing ionic strength mitigates the effects of electrostatic repulsion between the target DNA and probe DNA, thus also promoting the likelihood DNA hybridization.[30,34] We also chose buffers of high ionic strength and a PPM with relatively large (2 μm) pores to create a low ratio of surface-to-bulk charge in the PPM. The latter minimizes the effects of concentration polarization[35,36] and Donnan

exclusion[37,38] which can otherwise exclude the target from the affinity capture region. Our high ionic strength LE and TE also suppresses electroosmotic flow (EOF).[33,39]

We chose chloride as the LE ion because it is commonly found in significant amounts in many relevant biological samples (e.g., blood, urine, intra and extracellular fluids)[40] and has a high absolute electrophoretic mobility[41] (higher than nucleic acids[9]). As discussed by Rogacs et al., chloride is a particularly convenient LE ion for samples containing significant concentrations of chloride itself.[1] We chose HEPES as the TE ion since its absolute mobility is sufficiently low (in the presence of Tris as the counterion)[41] to focus DNA,[9] and yet is sufficiently high to exclude many matrix ions (e.g. PCR inhibitors found in blood).[1,7,42] Choosing a TE ion with absolute mobility closer to that of DNA would exclude more contaminants and would be associated with a lower smallness parameter ε (as per the analysis of Part I of this two-part series). However, this would also decrease the amount of analyte that can be extracted via semi-infinite injection ITP (see Section SI 1). Finally, Tris as a counterion to provided a pH of approximately 8.2 for the hybridization reaction, and hybridization of DNA occurs readily around this pH.[43,44]

SI 8. Analyses of ITP-AC purified 25 nt target from 10,000x contaminant via electrophoresis

We performed a series of experiments using electrophoresis to analyze our nucleic acid mixtures before and after purification. Figure S-4 shows electropherograms of (a) a trailing electrolyte containing 25 nt target and 10,000x more abundant (by mass) fish sperm DNA, (b) fish sperm DNA alone, (c) 25 nt target alone, and (d)-(f) eluted fractions from three separate ITP-AC experiments where 25 nt target was purified from 10,000x more abundant fish sperm DNA. All electropherograms were obtained using Agilent 2100 Bioanalyzer Instrument (Santa Clara, CA) using the Small RNA chip. The Bioanalyzer Small RNA chip can resolve nucleic acids in 6 to 150 nt range. In all electropherograms signal from the Agilent Bioanalyzer was normalized by the maximum signal of the sample. For experiments shown in (d)-(f) ITP-AC was performed as described in SI 7 and in sections 2.4 and 3.7 of the main text. Specifically, after the target was captured (Step 3, Figure 2b of main text) the LE and TE buffers were removed by vacuum. We then eluted the captured target by introducing (with a syringe) 5 µl elution buffer consisting of 50 mM sodium hydroxide. We used a syringe to drive this slug through the column and so elute the target. We quickly mixed the eluate with 5 µl of 200 mM HEPES to achieve a solution with near neutral pH. We then stored the purified sample at -20°C until analysis via the Bioanalyzer electrophoresis instrument. The electrophoresis on the Bioanalyzer instrument was performed by Stanford Protein and Nucleic Acid Facility. The resulting electropherograms corroborate our assertion that we purify target DNA. This evidence is presented in addition to the strong spectral evidence shown in Figure 5 of the main text. Together, these data show that ITP-AC reproducibly enriches the amount of 25 nt target and removes the majority of the background contaminant.

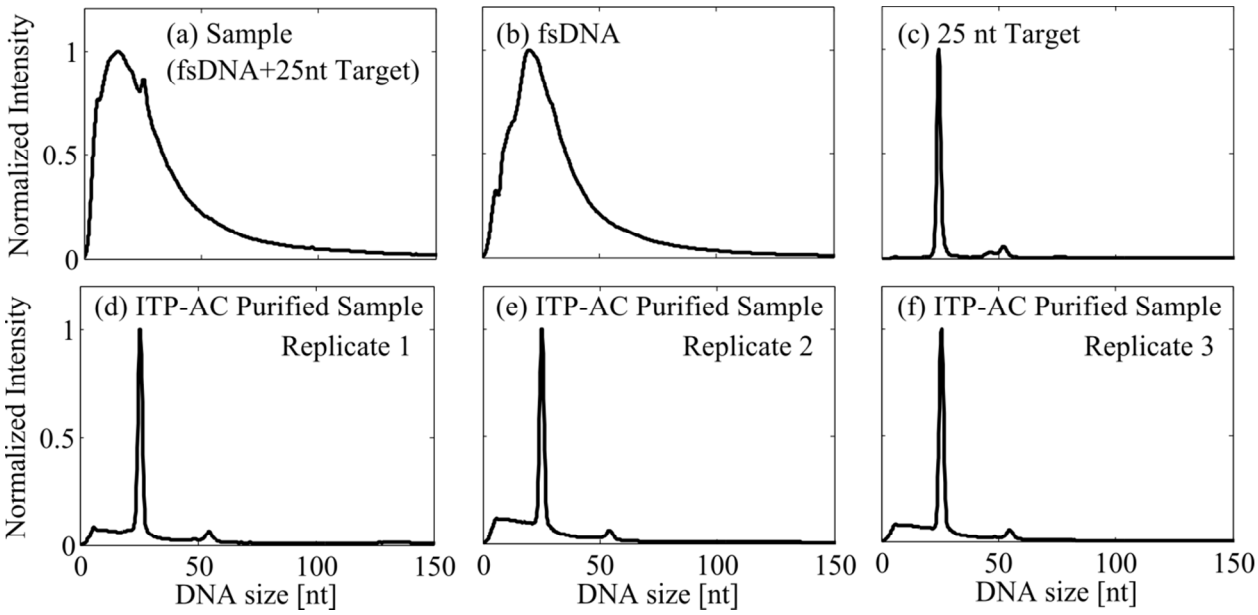

Figure S-4. Electropherograms of nucleic acid mixtures before and after application of our purification process. Shown are electropherograms of (a) mixture of trailing electrolyte (25 mM HEPES, 50 mM Tris) and 25 nt target and 10,000x more abundant (by mass) fish sperm DNA before purification, (b) fish sperm DNA alone (c) 25 nt target alone, and (d)-(f) three replicates of ITP-AC purified samples which initially contained 25 nt target and 10,000x more abundant fish sperm DNA. All electropherograms were obtained via Agilent Bioanalyzer Small RNA chip (6-150 nt range). In all electropherograms the signal from the Bioanalyzer instrument was normalized by the maximum signal for the sample. ITP-AC reproducibly enriches the amount of 25 nt target and removes the majority of the background contaminant.

SI 9. Recommended ITP-AC parameters

Here we provide a table of dimensional values of important ITP-AC parameters which we recommend for performing ITP-AC experiments. We also include brief rationale for each choice.

Table S1. Recommended ITP-AC parameters

Parameter	Value	Rationale
Affinity region pore size	0.1 - 2 μm	(a)
Affinity probe concentration, N	0.3-300 μM	(b)
Target-probe dissociation constant, K_d	$< 10^{-9}$ M	(c)
ITP channel diameter	100-5000 μm	(d)
Affinity region length	0.1-100 mm	(e)
ITP velocity, u	0.5-0.005 mm s^{-1}	(f)
Affinity region porosity, φ	0.5-0.8	(g)
Target diffusion coefficient, D	$< 10^{-9}$ m^2 s^{-1}	(h)

(a) We recommend that the PPM affinity region pore size be 10-100 times less than the radius of gyration of the target macromolecule so that the target is not mechanically sieved by the affinity

region.[45] For example, the radius of gyration of linearized λ phage DNA ranges from 0.18 μm for 4 kb strand to 2.5 μm for 309 kb strand.[46] For proteins, the radius of gyration typically ranges from 1.4 nm for 14 kDa protein (e.g., lysozyme from chicken egg white) to 6.4 nm for 820 kDa protein (α2-Myoglobin).[47] See Tyn and Gusek for a large table of radii of gyration for proteins.[47] However, we do not recommend using excessively large pores as this will lead to decreased affinity probe concentration (for a given probe surface density) and therefore decreased affinity column performance. Therefore an affinity region with a pore size of less than about 2 μm should successfully perform affinity capture on a wide range of biomolecules and bioparticles without sieving effects.

(b) As we mention in SI Section 6.3 we recommend DNA probe surface densities of around 2×10^{-12} molecules cm^{-2} as these give roughly the highest hybridization efficiencies per probe.[30] We recommend using the highest possible volumetric density of the probe (N) and therefore using the smallest affinity region pore size that will not cause sieving, concentration polarization or Donnan exclusion (see SI 7).

(c) We recommend that the non-dimensionalized target-probe dissociation constant β be less than about 10^{-5} as then the affinity reaction would appear irreversible, which is desired for effective capture of target (see Part I, Figure 4). While ITP-AC can purify targets with higher β, this is not desirable as capture of the target is not effective and may be non-specific (see Part I, Section 3.2.4). Therefore, if N is at least 10^{-4} M, we recommend that K_d, be less than about 10^{-9} M. Note that this is condition is satisfied by surface hybridization of oligonucleotides,[16,17] a large number of antibodies,[48] and a large number of aptamers.[49]

(d) The lower range of ITP channel diameters is limited by the integration of the porous affinity region. We recommend that ITP channel diameter be 10 to 100 times the affinity region pore diameter for adequate structural stability of the porous region. The upper range of ITP channel diameters is limited by the Joule heating in ITP and the stability of the ITP interface.[3,50]

(e) We recommend choosing an affinity region length based on the anticipated capture length. If saturation of the affinity region is not anticipated, this can be calculated using Equation (39) from Part I of this two part series. If saturation of the affinity region is anticipated, then the capture length is approximately equal to the target amount in the sample divided by the product of affinity region cross sectional area and affinity probe concentration. We recommend choosing affinity region length to be roughly twice the capture length as to capture the majority of the target while conserving space in the purification system.

(f) We recommend choosing ITP velocity during the hybridization phase based on the desired capture length, the forward rate constant of the target, and the probe density of the affinity region (see Equation (39), Part I). We note that the ITP velocity during the extraction phase can be (and likely should be) much higher than the velocity applied during the hybridization phase (see Figure 2 , Part 2) to minimize the overall assay time. The upper range of ITP velocities is limited

by excessive heating due to the proportionally higher current density needed to maintain higher ITP velocity. Excessive heating can lead to outgassing of the solvent for the LE and TE buffers, possibly solvent boiling, and even thermal damage to the target itself.[3] The lower range of ITP velocities is limited by the desired maximum width of the target distribution (and/or maximum assay time). The lower the ITP velocity, the larger the target distribution width[51,52] and therefore the gains of ITP preconcentration are diminished (see Figure 3, Part I).

(g) We recommend choosing an affinity region porosity in the range of 0.5-0.8. Porous materials with larger porosities require less pressure to fill the affinity region with the leading electrolyte and later the elution buffer.[29] Porous materials with larger porosities can also present more surface area per volume of material to the flow, potentially allowing for larger probe concentration. However, excessively large porosities cause the porous region to be structurally weak, and therefore difficult to work with.

(h) We recommend that, when using the model in Part I, and operating in the range of recommended parameters that the target diffusion constant be less than 10^{-9} m^2 s^{-1} so that the target diffusion will be negligible compared to target migration (see Part I, Equation (20)). This is easily satisfied for a majority of biomolecules and even viruses. For example, for DNA oligonucleotides diffusion constant is order 10^{-10} m^2 s^{-1}.[53] For larger DNA, for example, for linearized λ phage DNA, the diffusion constant ranges from 2×10^{-12} m^2 s^{-1} for 4 kb strand to 2×10^{-13} m^2 s^{-1} for 309 kb strand.[46] For proteins, the diffusion constant typically ranges from 1.1×10^{-10} m^2 s^{-1} for 14 kDa protein (e.g., lysozyme from chicken egg white) to 2.4×10^{-11} m^2 s^{-1} for 820 kDa protein (α2-Myoglobin).[47] For viruses the diffusion constant ranges from 1.5×10^{-11} m^2 s^{-1} for 5,000 kDa Bromegrass mosaic virus to 5×10^{-12} m^2 s^{-1} for 50,000 kDa Tobacco mosaic virus. See Tyn and Gusek for an extensive and useful table of diffusion constants for proteins and viruses.[47]

References

(1) Rogacs, A.; Marshall, L. A.; Santiago, J. G. *J. Chromatogr. A* **2014**, *1335*, 105-120.
(2) Boček, P.; Deml, M.; Kaplanová, B.; Janák, J. *J. Chromatogr. A* **1978**, *160*, 1-9.
(3) Marshall, L. A. *Designing automated systems for sample preparation of nucleic acids using isotachophoresis*, 2013.
(4) Shkolnikov, V.; Santiago, J. G. *Lab Chip* **2013**, *13*, 1632-1643.
(5) Persat, A.; Suss, M. E.; Santiago, J. G. *Lab Chip* **2009**, *9*, 2454-2469.
(6) Everaerts, F. M.; Beckers, J. L.; Verheggen, T. P. E. M. *Isotachophoresis: Theory, Instrumentation, and Applications*; Elsevier: Amsterdam, New York, 1976.
(7) Persat, A.; Marshall, L. A.; Santiago, J. G. *Anal. Chem.* **2009**, *81*, 9507-9511.
(8) Bercovici, M.; Lele, S. K.; Santiago, J. G. *J. Chromatogr. A* **2009**, *1216*, 1008-1018.
(9) Stellwagen, N. C.; Gelfi, C.; Righetti, P. G. *Biopolymers* **1997**, *42*, 687-703.
(10) Polyanskiy, M. N. *Refractive Index Database*. http://refractiveindex.info, 2008.
(11) Thomas, S. W.; Joly, G. D.; Swager, T. M. *Chem. Rev.* **2007**, *107*, 1339-1386.

(12) Lakowicz, J. R. *Principles of Fluorescence Spectroscopy*, 3 ed.; Springer New York, 2006.
(13) Markham, N. R.; Wright, A.; Zuker, L. S.; Zuker, M. *The UNAFold Web Server*. http://mfold.rna.albany.edu/, 1995.
(14) Erickson, D.; Li, D.; Krull, U. J. *Anal. Biochem.* **2003**, *317*, 186-200.
(15) Levicky, R.; Horgan, A. *Trends Biotechnol.* **2005**, *23*, 143-149.
(16) Stevens, P. W.; Henry, M. R.; Kelso, D. M. *Nucleic Acids Res.* **1999**, *27*, 1719-1727.
(17) Okahata, Y.; Kawase, M.; Niikura, K.; Ohtake, F.; Furusawa, H.; Ebara, Y. *Anal. Chem.* **1998**, *70*, 1288-1296.
(18) Schwarzenbach, H.; Hoon, D. S.; Pantel, K. *Nat. Rev. Cancer* **2011**, *11*, 426-437.
(19) West, J. A.; Satterfield, B. C. In *Microchip-Based Assay Systems*; Springer, 2007, pp 9-21.
(20) Ma, J.; Zhang, L.; Liang, Z.; Zhang, W.; Zhang, Y. *J. Sep. Sci.* **2007**, *30*, 3050-3059.
(21) Sinitsyna, E. S.; Walter, J. G.; Vlakh, E. G.; Stahl, F.; Kasper, C.; Tennikova, T. B. *Talanta* **2012**, *93*, 139-146.
(22) Křvenková, J.; Bilková, Z.; Foret, F. *J. Sep. Sci.* **2005**, *28*, 1675-1684.
(23) Mallik, R.; Hage, D. S. *J. Sep. Sci.* **2006**, *29*, 1686-1704.
(24) Rohr, T.; Yu, C.; Davey, M.; Svec, F.; Fréchet, J. *Electrophoresis* **2001**, *22*, 3959.
(25) Yu, C.; Xu, M.; Svec, F.; Frecht, J. M. J. *J. Polym. Sci. A1.* **2002**, *40*, 755-769.
(26) Yu, C.; Svec, F.; Fréchet, J. M. J. *Electrophoresis* **2000**, *21*, 120-127.
(27) Yu, C.; Davey, M. H.; Svec, F.; Fréchet, J. M. *Anal. Chem.* **2001**, *73*, 5088-5096.
(28) Podgornik, A.; Jančar, J.; Merhar, M.; Kozamernik, S.; Glover, D.; Čuček, K.; Barut, M.; Štrancar, A. *J. Biochem. Bioph. Methods* **2004**, *60*, 179-189.
(29) Shkolnikov, V.; Strickland, D. G.; Fenning, D. P.; Santiago, J. G. *Sensor. Actuat. B-Chem.* **2010**, *150*, 556-563.
(30) Peterson, A. W.; Heaton, R. J.; Georgiadis, R. M. *Nucleic Acids Res.* **2001**, *29*, 5163-5168.
(31) Bocek, P. *Analytical Isotachophoresis*; VCH: Cambridge, 1987.
(32) Hruška, V.; Gaš, B. *Electrophoresis* **2007**, *28*, 3-14.
(33) Kirby, B. J.; Hasselbrink, E. F. *Electrophoresis* **2004**, *25*, 187-202.
(34) Špringer, T.; Šípová, H.; Vaisocherová, H.; Štěpánek, J.; Homola, J. *Nucleic Acids Res.* **2010**, *38*, 7343-7351.
(35) Mani, A.; Zangle, T. A.; Santiago, J. G. *Langmuir* **2009**, *25*, 3898-3908.
(36) Zangle, T. A.; Mani, A.; Santiago, J. G. *Langmuir* **2009**, *25*, 3909-3916.
(37) Waki, H.; Tokunaga, Y. *J. Liq. Chromatogr.* **1982**, *5*, 105-119.
(38) Waki, H.; Tokunaga, Y. *J. Chromatogr. A* **1980**, *201*, 259-264.
(39) Kirby, B. J.; Hasselbrink, E. F. *Electrophoresis* **2004**, *25*, 203-213.
(40) Costanzo, L. S. *Physiology*, 4th ed.; Saunders, 2009.
(41) Hirokawa, T.; Nishino, M.; Aoki, N.; Kiso, Y.; Sawamoto, Y.; Yagi, T.; Akiyama, J. I. *J. Chromatogr. A* **1983**, *271*, D1-D106.
(42) Wilson, I. G. *Appl. Environ. Microbiol.* **1997**, *63*, 3741.
(43) Edman, C. F.; Raymond, D. E.; Wu, D. J.; Tu, E.; Sosnowski, R. G.; Butler, W. F.; Nerenberg, M.; Heller, M. J. *Nucleic Acids Res.* **1997**, *25*, 4907-4914.
(44) Wetmur, J. G. *Annu. Rev. Biophys. Bioeng.* **1976**, *5*, 337-361.
(45) Völkel, A. R.; Noolandi, J. *Electrophoresis* **1995**, *16*, 2086-2093.
(46) Smith, D. E.; Perkins, T. T.; Chu, S. *Macromolecules* **1996**, *29*, 1372-1373.
(47) Tyn, M. T.; Gusek, T. W. *Biotechnol. Bioeng.* **1990**, *35*, 327-338.
(48) Abcam. *KD value: A quantitative measurement of antibody affinity*. http://www.abcam.com/index.html?pageconfig=resource&rid=15749, 2014.

(49) Lollo, B.; Steele, F.; Gold, L. *Proteomics* **2014**.
(50) Hirokawa, T.; Kiso, Y. *J. Chromatogr. A* **1994**, *658*, 343-354.
(51) Shkolnikov, V.; Bahga, S. S.; Santiago, J. G. *PCCP* **2012**, *14*, 11534–11545.
(52) MacInnes, D. A.; Longsworth, L. G. *Chem. Rev.* **1932**, *9*, 171-230.
(53) Stellwagen, E.; Stellwagen, N. C. *Electrophoresis* **2002**, *23*, 2794-2803.